J Mater Sci (2007) 42:6803–6808
DOI 10.1007/s10853-006-1400-1

Properties of barium-strontium titanate PTCR ceramics sintered on different powder beds

Pornsuda Bomlai · Steven J. Milne

Received: 8 May 2006 / Accepted: 4 December 2006 / Published online: 26 April 2007

Abstract Barium-strontium titanate (BST) ceramics, co-doped with Sb and Mn oxides, were sintered on different powder beds: Sb-doped BST; Al_2O_3; or Sb,Mn-codoped BST powder. Phase formation, microstructure and the electrical properties of the samples were analysed. The PTCR behavior depended significantly on the type of powder bed used. The BST ceramic pellet sintered on the Sb-BST powder displayed the largest PTCR effect, with a ρ_{max}/ρ_{RT} ratio of ~10^6. This was an order of magnitude greater than for samples sintered on the other two powders. Complex impedance analysis confirmed that this was due to a large increase in grain boundary resistance at 250 °C.

Introduction

It is well known that donor-doped barium titanate ($BaTiO_3$)-based ceramics exhibit positive temperature coefficient of resistivity (PTCR) behavior, and are widely used as over-current protection devices, self-regulating heaters, and temperature sensors in electronic circuits [1]. This behaviour was discovered in 1955 and refers to an abnormal increase of resistivity around the Curie temperature (T_C) [2–3]. The T_C can be shifted to lower temperatures by adding $SrTiO_3$ forming a solid solution of barium-strontium titanate ($(Ba_{1-x}Sr_x)TiO_3$, BST) [4].

P. Bomlai (✉)
Materials Science Program, Faculty of Science,
Prince of Songkla University, Songkhla 90112, Thailand
e-mail: ppornsuda@yahoo.com

S. J. Milne
Institute for Materials Research, University of Leeds,
Leeds LS2 9JT, UK

The most accepted conduction models to explain the sudden change of resistivity have been proposed by Heywang and Jonker; a potential barrier arises from the electron-trapping effect of surface acceptor states at grain boundary regions leading to high resistivity in the materials immediately above T_C [5–6]. The lower resistivity of the materials at temperatures below T_C, results from the compensation of surface states due to spontaneous polarization which occurs within ferroelectric domains.

Low resistivity at room temperature and a strong PTCR effect, $\rho_{max}/\rho_{RT,}$ are both critical parameters for device applications. It is reported that the PTCR characteristics of $BaTiO_3$-based ceramics are very sensitive to both the microstructure and the defect chemistry of the materials, which are strongly influenced by processing parameters such as chemical composition, and sintering conditions [7–9]. Recently, a new process for introducing a donor dopant the so-called vapour-doping method, involving doping with a vapour of a dopant oxide e.g. Bi_2O_3, Sb_2O_3 or B_2O_3 during sintering, has also been demonstrated to lead to a significant improvement in the PTCR effect [10–15]. Therefore, it is important to consider the possible effect on PTCR properties of any volatile oxides contained in the powders on which pellets are placed during sintering. The objective of this study was to investigate the effects of three different powder-bed compositions on phase formation, electrical properties and microstructures of Sb, Mn-modified BST ceramics. The powder beds were: Sb_2O_3-doped BST; alumina; and BST co-doped with Sb_2O_3 and MnO_2.

Experimental procedure

Samples in this work were prepared by using the conventional mixed oxide process. Starting materials were $BaCO_3$,

$SrCO_3$, TiO_2, Sb_2O_3, SiO_2 and MnO_2 (Aldrich Chemical Company, Inc., 99.9+% purity) which were mixed in a ratio to produce the composition [$(Ba_{0.8}Sr_{0.2})TiO_3$ + 0.15 mol% Sb_2O_3 + 1.0 mol% TiO_2 + 3.0 mol% SiO_2 + 0.005 mol% MnO_2]. Silica and titania were added to enhance sintering behaviour; this composition is referred to as Sb,Mn doped BST. After ball-milling with zirconia grinding media and ethanol in a polypropylene jar for 24 h, the mixture was dried, ground and then calcined in air at 1100 °C for 2 h. The calcined powder was blended with 3 wt.% polyvinyl alcohol (PVA) and then pressed into pellets 15 mm in diameter.

Pellets were sintered on three types of powder bed in an alumina crucible: (a) Sb-doped BST powder; (b) alumina powder (as a 'control') and (c) Sb, Mn-doped BST powder. Specifically, the BST powder bed compositions were (a) $(Ba_{0.8}Sr_{0.2})TiO_3$ + 1.0 mol% TiO_2 + 0.15 mol%Sb_2O_3; (c) $(Ba_{0.8}Sr_{0.2})TiO_3$ + 1.0 mol% TiO_2 + 0.15 mol% Sb_2O_3 + 0.005 mol% MnO_2. All of the samples were sintered in an air atmosphere at 1350 °C, using heating and cooling rates of 5 °C/min. To examine any variability in the data, duplicate samples were sintered under the same conditions and two pellets from each experiment were selected for characterization.

Phase formation in sintered samples was analyzed at room temperature using an X-ray diffraction technique (XRD), with CuK_α radiation (Philips APD1700); polished surfaces were analysed. The lattice parameters were calculated using a least square fitting program which 2θ scanned at lower speed of 0.004 deg/s [16]. The microstructures of the as-sintered surfaces of the samples were characterized using scanning electron microscopy (ESEM, Phillips XL30). The d.c. resistance change of the specimens as a function of temperature was measured using a digital multimeter (Agilent 34401A) and a suitable power supply; electrodes were applied using silver paste. The measurements were carried out from room temperature to ~320 °C using a silicone oil bath to heat the samples; a digital thermometer (Fluke S50) with a K-type thermocouple was used to monitor temperature. The impedance analysis was carried out using an impedance analyzer (HP 4192A) at a signal strength of 0.5 V, with various frequencies ranging from 5 Hz to 13 MHz. Measurements were carried out at room temperature and 250 °C.

Results and discussion

XRD patterns for each sintered sample are shown in Fig. 1. The tetragonal barium strontium titanate (BST) phase was indexed on the basis of the Joint Committee on Powder Diffraction Standards (JCPDS) data [17]. The tetragonal peak splitting was only evident at high angles [18]. The *a* and *c* lattice parameters of the samples for each of the three powder beds were as follows: Sb-BST, a = 3.972 Å, c = 3.990 Å; Al_2O_3, a = 3.975 Å, c = 3.992 Å; Sb,Mn-BST, a = 3.972 Å, c = 3.989 Å. Minor phases were present in all three samples. The d-spacings of these minor phases were consistent with phases previously identified with the aid of EPMA to be $(Ba,Sr)_6Ti_{17}O_{40}$ (with ~1 mol% Sr^{2+} for Ba^{2+} substitution) and $Ba_{1.95}Sr_{0.05}Ti_{1.2}Si_{1.8}O_8$ which segregate at intergranular regions [18, 19].

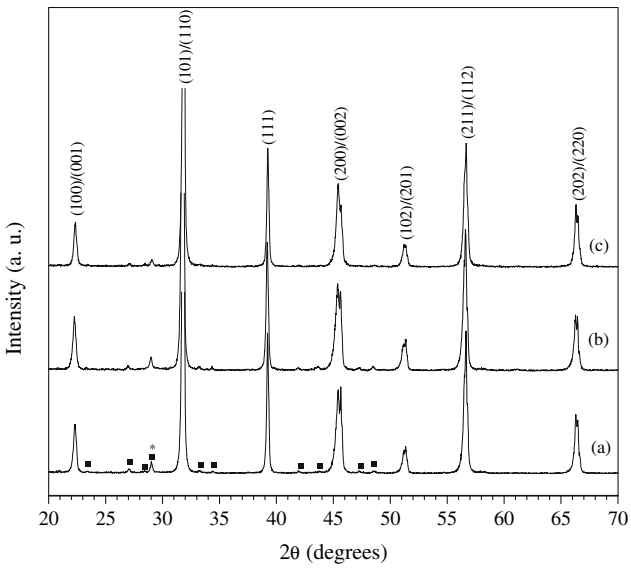

Fig. 1 X-ray diffraction patterns of sintered ceramics showing phase formation with different powder beds during sintering; (**a**) Sb-doped BST powder, (**b**) alumina powder and (**c**) Sb, Mn-doped BST powder (* = $(Ba,Sr)_6Ti_{17}O_{40}$ and ■ = $Ba_{1.95}Sr_{0.05}Ti_{1.2}Si_{1.8}O_8$)

The resistivities (ρ) of the samples as a function of temperature for the three different powder beds are potted in Fig. 2; results are summarised in Table 1. All samples exhibited PTCR behavior with the onset temperature of the sharp rise in resistance remaining constant at ~60 °C, corresponding to the Curie temperature for this composition. There was little variation in room temperature resistivity (ρ_{RT}) for the different samples, with values of 162, 177 and 164 Ω cm for Sb-BST, Al_2O_3 and Sb,Mn-BST respectively. The temperature of maximum resistivity (T_{max}) was 256–258 °C for Sb-BST and Sb,Mn-BST beds. For Al_2O_3, the peak in Fig. 2 was broader, with ρ_{max} at ~300 °C. A key factor in PTCR performance is the ratio of maximum resistivity and room temperature resistivity, ρ_{max}/ρ_{RT}. The ratio for ceramics sintered on the Sb-doped powder was ~1×10^6, which is an order of magnitude higher than for the other powder beds. The higher ratio stemmed from the increased value of maximum resistivity, 1.7×10^8 Ω cm, for the Sb-BST powder bed, Table 1.

More detailed information on the electrical properties of the samples was obtained from complex impedance

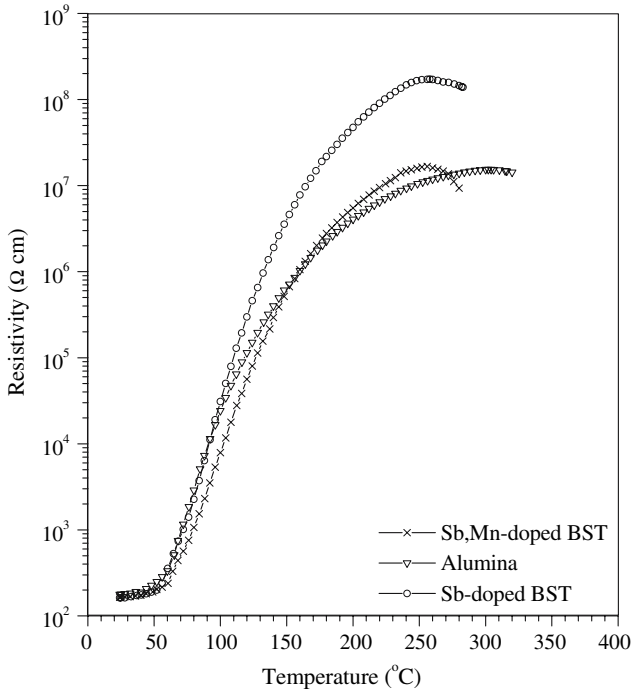

Fig. 2 The resistivity-temperature characteristics of the samples for various powder beds during sintering at 1350 °C

Table 1 Summary of values of room temperature resistivity (ρ_{RT}), maximum resistivity (ρ_{max}), the ratio ρ_{max}/ρ_{RT} and the temperature corresponding to ρ_{max} (T_{max})

Samples	ρ_{RT} (Ω cm)	ρ_{max} (Ω cm)	ρ_{max}/ρ_{RT}	T_{max} (°C)
A	162	1.73×10^8	1.07×10^6	258
B	177	1.53×10^7	8.64×10^4	302
C	164	1.67×10^7	1.02×10^5	256

spectroscopy. A polycrystalline ceramic (with non blocking electrodes) can generally be represented by an equivalent circuit of a series array of two parallel RC elements [20], one RC element representing the grains and the other the grain boundaries (Fig. 3). Depending on the relative values of resistance and capacitance in each RC element, two semicircles may appear in plots of the real part (Z') of complex impedance versus the imaginary part

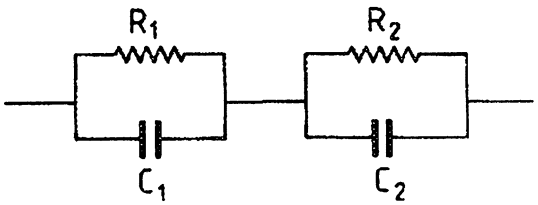

Fig. 3 Equivalent circuit used to represent the electrical properties of bulk and grain boundary effects in PTCR $BaTiO_3$ [20] (R_1, C_1 = grain boundary resistance (R_{gb}) and capacitance (C_{gb}); R_2, C_2 = grain resistance (R_g) and capacitance (C_g) respectively)

(Z''); one for each RC element. However whether or not each semi-circle is represented at a given temperature, and frequency range, depends on the relative values of R and C in each circuit element. Resistance values can be abstracted from the intercepts with the real axis. Figure 4 show plots of Z' vs Z'', measured at room-temperature and 250 °C, for each of the three sample-types. These two temperatures correspond approximately to the positions of ρ_{RT} and ρ_{max} for the two BST powder bed compositions (Fig. 2).

The complex impedance plot at room temperature, Fig. 4a, shows a distorted semi-circle with a non-zero high frequency intercept. The low frequency intercept represents R_T the total resistance ($R_{gb} + R_g$); the high-frequency intercept represents R_g. The latter value, was ~4–5 Ω for all three powder beds, consistent with semiconducting grains. Because of the low resistance grains, only one semi-circle was present, the higher resistance grain boundary element of the equivalent circuit dominating the impedance plot, Fig. 4a. The grain boundaries were also of comparatively low resistance, as expected at room-temperature for this particular BST composition (Fig. 2). Values ranged from 20 Ω for Sb-BST to 26 Ω, for the alumina powder bed.

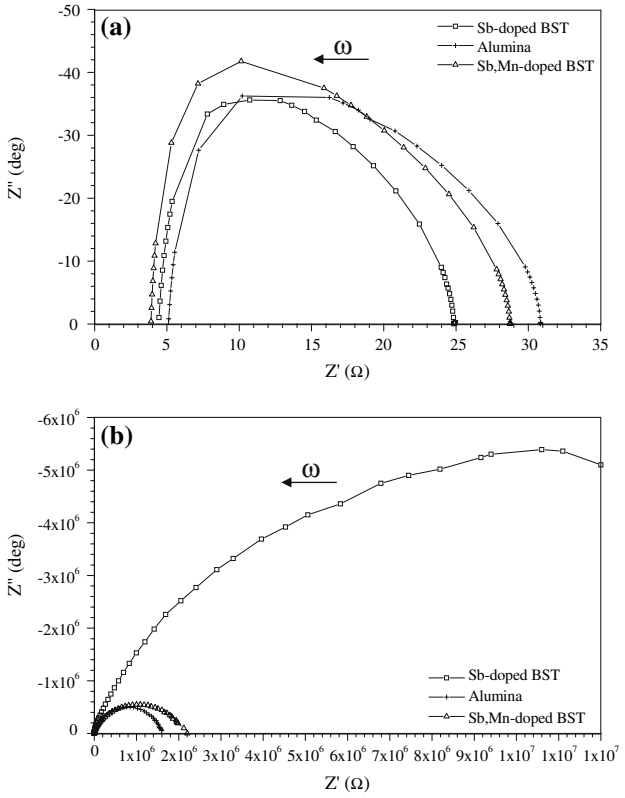

Fig. 4 Impedance spectra of sintere samples with different powder beds during sintering at 1350 °C, as recorded at room temperature (**a**) and 250 °C (**b**)

Impedance measurements at 250 °C, again revealed single semi-circles in Z' vs Z'' plots. Non-linear high frequency intercepts gave R_g values similar to those at room-temperature, i.e. a few ohms, confirming semi-conducting behavior, Fig. 4b. For alumina and the Sb, Mn co-doped powder bed samples, the full semi-circle fell within the frequency range of measurement. The semi-circles were not distorted. Only part of the semi-circle appeared for Sb-BST from which an estimated value of $R_{gb} + R_g$ could be found by extrapolation. The resulting R_{gb} value was $\sim 2 \times 10^7$ Ω for the Sb-BST powder, an order of magnitude higher than for the other two samples, each of which had R_{gb} values of $\sim 2 \times 10^6$ Ω. This is in contrast to the room-temperature results where all three samples had exhibited similar R_{gb} values.

In order to gain a further understanding of the ac response, and to investigate if other grain boundary RC elements may be present with similar capacitances, the Modulus formalism was investigated, at 250 °C [20]. Plots of M' vs. M'' are shown in Fig. 5. Each sample gave a single-semi circle, consistent with an equivalent circuit containing one $R_{gb}C_{gb}$ element. This was also true for the room-temperature data, Fig. 5. Capacitance values abstracted from intercepts with the M' axis (ε_o/C) gave $C_{gb} = 3.9 \times 10^{-9}$ F/cm, at 250 °C, for Sb-doped BST powders. The grain boundary capacitances of the other two samples at 250 °C were 4–5 times smaller. At room-temperature the respective capacitances were an order of magnitude smaller than the 250 °C data, for example using Sb-BST powder $C_{gb} = 3.4 \times 10^{-10}$ F/cm.

Spectroscopic plots of M'' and Z'' vs. frequency are shown in Figs. 6 and 7. At room temperature the M'' and Z'' peaks occurred over a narrow frequency range for all samples. The peak heights of the Z''-f peaks were similar, Fig. 7, and the peaks occurred at similar frequencies, as expected from the similarity in values of R_{gb} abstracted from Z' vs. Z'' plots. The peak heights of the M'' peaks were also in agreement with the relative values of C_{gb} taken from M' vs. M'' plots. In M''-f plots the larger the capacitance the smaller the peak and the lower its frequency. Hence the Sb-BST powder bed gave rise to a M''-f peak around half the intensity of the other two sample-types, and the frequency of the peak maximum was slightly lower, Fig. 6a.

At 250 °C the height of the M'' peak in the M''-f plot for the Sb-BST powder bed, was in proportion to the 4-5-fold difference in C_{gb} taken from M' vs. M'' plots. The higher impedance of the Sb-BST at 250 °C gave rise to a

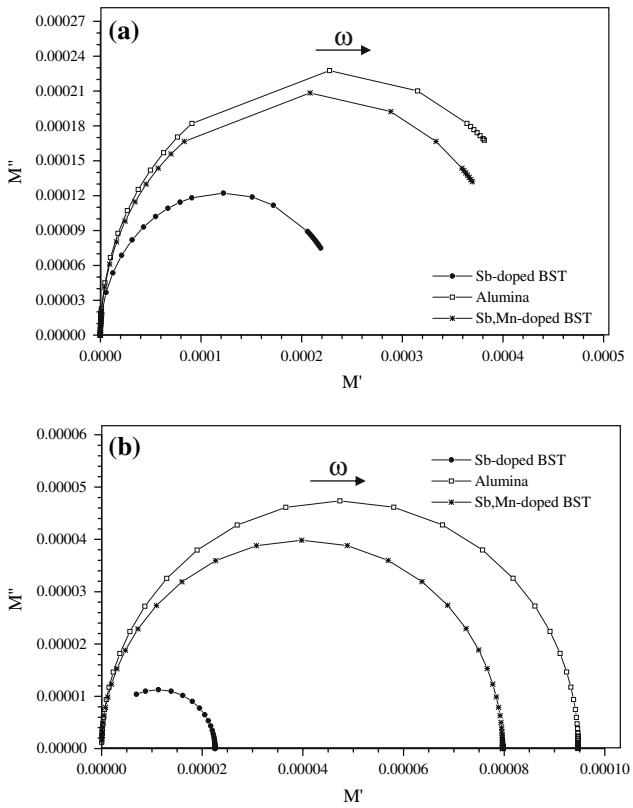

Fig. 5 Complex modulus plane plots of sintered samples with different powder beds during sintering at 1350 °C, as recorded at room temperature (**a**) and 250 °C (**b**)

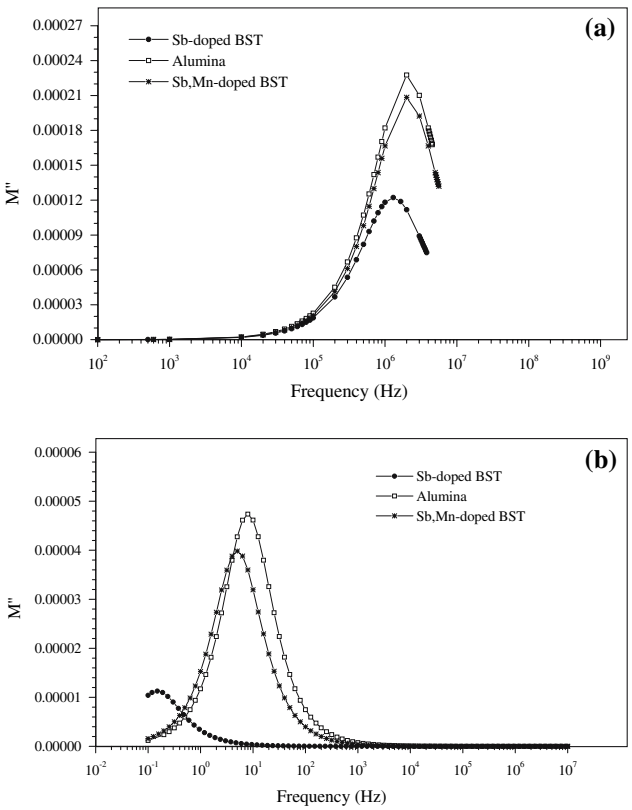

Fig. 6 Modulus M'' spectroscopic plots of sintered samples with different powder beds during sintering at 1350 °C, as recorded at room temperature (**a**) and 250 °C (**b**)

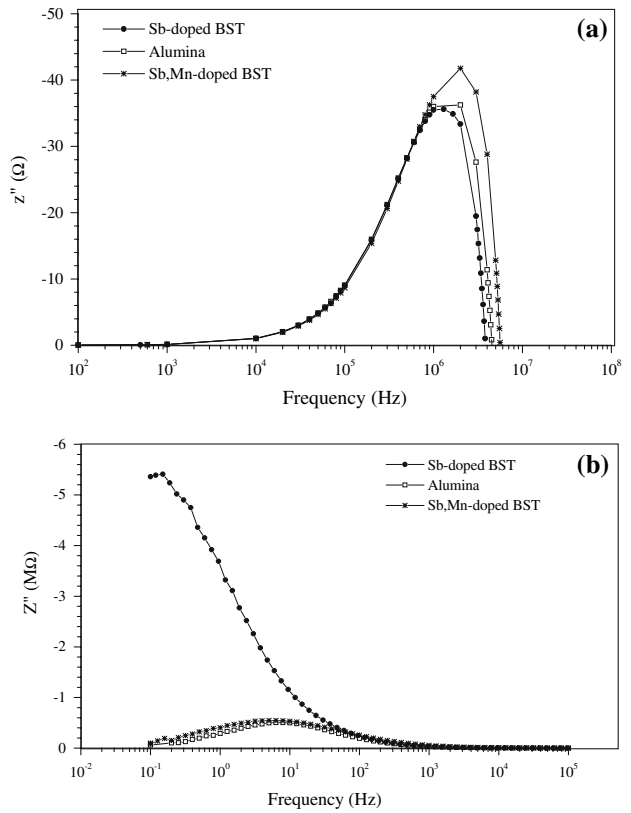

Fig. 7 Impedance Z'' spectroscopic plots of sintered samples with different powder beds during sintering at 1350 °C, as recorded at room temperature (**a**) and 250 °C (**b**)

dominant peak in the Z''-f plot. Because of the higher grain boundary impedance (Fig. 4 (Z'-Z'') at 250 °C, and the much higher grain boundary capacitance, the peaks in M''-f and Z''-f plots for the Sb-BST powder bed at 250 °C were shifted to much lower frequency than had been the case at room temperature.

Overall, the impedance and modulus analysis of this BST PTCR ceramic sintered on different powder beds reveal that the increase in ρ_{max} (at ~250 °C) first observed from dc measurements (Fig. 2) was due to a substantial increase in grain boundary resistance (height of Schottky barriers) for the Sb-BST powder bed sample. The measurements also revealed an increase in grain boundary capacitance in this sample. The ratio of the area and thickness of the sintered pellets gave a cell constant of ~6.5 cm for all pellets, hence resistance values quoted in the above text give a close correspondence to dc resistivity values shown in Table 1.

Changes in electrical properties of the pellets as a result of changing the powder bed may be attributed to differences in the net gain of volatile Sb and Mn oxides which are generated by evaporation from the high surface area powder beds. Diffusion of vapours, along grain boundaries could lead to a net increase in dopant concentration at grain interfaces. Consequently, interfacial defect chemistry would be modified. Indeed Qi et al. [14] have suggested that an effective means of introducing Sb_2O_3 as a donor dopant for the purpose of creating A site vacancies on the ABO_3 perovskite lattice of BST is through a vapour phase reaction. The higher value of resistivity, ρ_{max} (at ~250 °C) of the sample sintered on Sb-BST powders is shown by impedance analysis to be due to an increase in grain boundary resistivity. The increased grain boundary capacitance of this sample is also indicative of changes to the grain boundary composition. The high capacitance value most probably is due to a higher dielectric constant in the interfacial region in this sample, as there was little change in microstructure (see below) between the Sb-BST and Al_2O_3 powder beds. Hence the total area of the grain-interface was similar, and it is difficult to see how there would be a decrease in the width of the grain boundary region, which could contribute to a large increase in C_{gb}.

In each of the samples the pellet surface in contact with the powder bed was removed by polishing before measuring the PTCR responses, therefore any solid state diffusion between the powder beds and the BST pellets is unlikely to affect the PTCR results. Removal of any reaction layer makes Al_2O_3 a useful point of comparison for the two BST powders. Both BST powders contained a small amount of TiO_2, but this is not volatile and would not affect the PTCR response in the ceramic. The powder bed containing Sb,Mn co-doped BST did not give rise to any significant increase in resistance at 250 °C, and its PTCR performance was similar to the 'control' sample sintered on Al_2O_3. This was despite similar amounts of Sb_2O_3 in both BST powder beds. Manganese oxide is also expected to be volatile at the sintering temperature (1350 °C). However it is generally considered to be an acceptor dopant in perovskites such as BST. Therefore the difference in PTCR data between samples sintered on Sb-doped and on Sb,Mn co-doped BST powders infers that in the latter, both oxide vapours diffuse along grain boundaries, but as one (Mn) is an acceptor and the other (Sb) a donor there is no overall change in electronic properties of the interfacial region. Hence little change in grain boundary resistance results.

The microstructures of as-sintered surface of all samples are shown in Fig. 8. The Sb-BST and the Al_2O_3 samples each had similar grain sizes, 12.6 ± 2.5 μm and 13.4 ± 5.0 μm respectively, whilst the Sb,Mn co-doped sample had a smaller average grain size, 8.2 ± 2.6 μm. The co-doped BST powder bed sample would therefore have a higher total surface area of grain boundaries, facilitating vapour diffusion (the densities of all samples were similar). Manganese is a well-known grain growth inhibitor in titanate perovskites, and the reduced grain size for the Sb, Mn powder bed sample is evidence that manganese oxide vapours were transported along grain boundaries, resulting

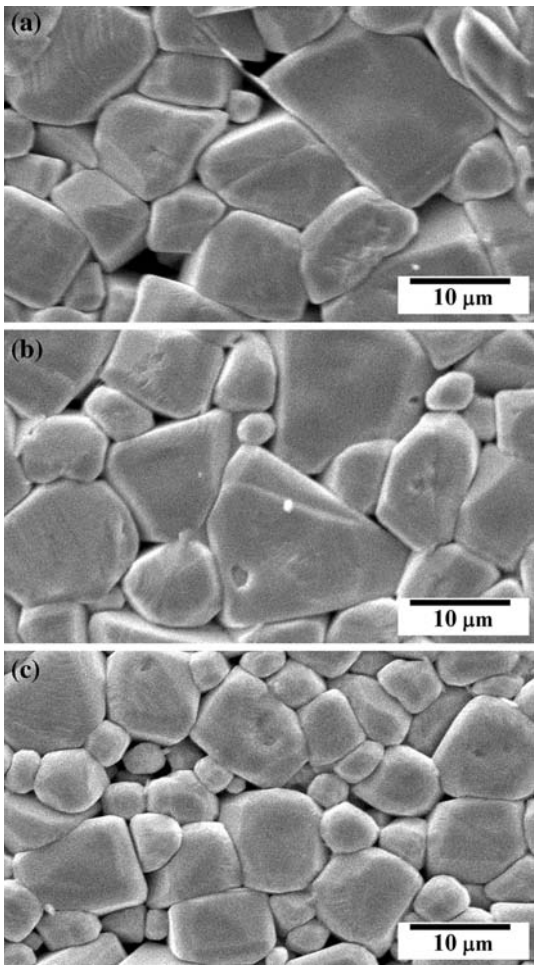

Fig. 8 SEM micrographs of as-sintered surfaces of samples sintered at 1350 °C with different powder beds during sintering; (**a**) Sb-doped BST powder, (**b**) alumina powder and (**c**) Sb, Mn-doped BST powder

in grain growth suppression. It has previously been reported that the uniformity of the microstructure significantly affects the electrical properties [21] and performance of PTCR devices. However the present results show changes in the PTCR effect arising predominantly from changes to the grain boundary resistance as a consequence of antimony oxide vapours, generated from the powder bed, altering the defect chemistry of the grain interfaces.

Conclusions

The composition of the powder bed has an important effect on the PTCR properties of BST ceramics. The PTCR effect is distinctly enhanced by using a suitable powder bed during the sintering process. The use of an Sb-doped BST powder to support the pellet during sintering raises the value of ρ_{max} (at ~250 °C), relative to samples set on alumina powder, or indeed on Sb and Mn codoped BST powder. Consequently a six-orders of magnitude increase in the PTCR effect, ρ_{max}/ρ_{RT}, is attained using the Sb-BST powder bed. This is ten times higher than for the other powder-beds. The higher PTCR effect using Sb-BST powders is attributed to diffusion of antimony oxide vapour along grain boundaries, leading to an increase in grain boundary resistance. The absence of any enhancement for co-doped Sb,Mn powder beds is suggested to be due to the compensating effect of manganese oxide vapours. A reduced grain size using the Sb,Mn co-doped powder bed was consistent with an increase in the Mn content at grain boundaries, suppressing grain growth.

Acknowledgements The authors would like to express their sincere thanks to P. Vogel and Electroceramics Laboratory in Chiang Mai University for impedance measurement.

References

1. He Z, Ma J, Qu Y, Feng X (2002) J Eur Ceram Soc 22:2143
2. Goodman G (1963) J Am Ceram Soc 46:48
3. Urek S, Drofenik MM (1999) J Eur Ceram Soc 19:913
4. Zhao J, Li L, Gui Z (2001) Sens Actuators A 95:46
5. Hewang W (1964) J Am Ceram Soc 47:484
6. Jonker GH (1964) Solid State Electron 8:895
7. Lin T-F, Hu C-T, Lin I-N (1990) J Am Ceram Soc 73:531
8. Ihrig H (1981) J Am Ceram Soc 64:617
9. Basu RN, Maiti HS (1987) Mater Lett 5:99
10. Qi J, Chen W, Wu Y, Li L (1998) J Am Ceram Soc 81:437
11. Chatterjee S, Maiti HS (2001) Mater Chem Phys 67:294
12. Qi J, Gui Z, Wang Y, Wu Y, Li L (2002) Mater Sci Eng B 95:283
13. Qi J, Gui Z, Zhu Q, Wang Y, Wu Y, Li L (2002) Sens Actuators A 100:244
14. Qi J, Gui Z, Wu Y, Li L (2001) Sens Actuators A 93:84
15. Qi J, Qing Z, Wang Y, Wu Y, Li L (2001) Solid State Commun 120:505
16. Holland TJB, Redfern SAT (1997) Mineral Magazine 61:65
17. Joint Committee for Powder Diffraction standard (JCPDS), card No. 44-0093
18. Bomlai P, Sirikulrat N, Brown A, Milne SJ (2005) J Eur Ceram Soc 25:1905
19. Bomlai P, Sirikulrat N, Brown A, Conliffe E, Milne SJ (2006) J Mater Sci 42:2175
20. Sinclair DC, West AR (1989) J Appl Phys 3850
21. Bomlai P, Sirikulrat N, Tunkasiri T (2005) Mater Lett 59:118